

Fermi-level pinning of bilayer graphene with defects under an external electric field

Ken Kishimoto and Susumu Okada

Citation: *Appl. Phys. Lett.* **110**, 011601 (2017); doi: 10.1063/1.4973426

View online: <http://dx.doi.org/10.1063/1.4973426>

View Table of Contents: <http://aip.scitation.org/toc/apl/110/1>

Published by the American Institute of Physics

Articles you may be interested in

[Self-forming graphene/Ni patterns on sapphire utilizing the pattern-controlled catalyst metal agglomeration technique](#)

Appl. Phys. Lett. **110**, 013103013103 (2017); 10.1063/1.4973523

[Impact of N-plasma and Ga-irradiation on MoS₂ layer in molecular beam epitaxy](#)

Appl. Phys. Lett. **110**, 012101012101 (2017); 10.1063/1.4973371

[Universal conformal ultrathin dielectrics on epitaxial graphene enabled by a graphene oxide seed layer](#)

Appl. Phys. Lett. **110**, 013106013106 (2017); 10.1063/1.4973200

[Fabrication of mirror templates in silica with micron-sized radii of curvature](#)

Appl. Phys. Lett. **110**, 011101011101 (2017); 10.1063/1.4973458



**THE WORLD'S RESOURCE FOR
VARIABLE TEMPERATURE
SOLID STATE CHARACTERIZATION**



WWW.MMR-TECH.COM

OPTICAL STUDIES SYSTEMS SEEBECK STUDIES SYSTEMS MICROPROBE STATIONS HALL EFFECT STUDY SYSTEMS AND MAGNETS

Fermi-level pinning of bilayer graphene with defects under an external electric field

Ken Kishimoto^{a)} and Susumu Okada^{b)}

Graduate School of Pure and Applied Sciences, University of Tsukuba, 1-1-1 Tennodai, Tsukuba, Ibaraki 305-8571, Japan

(Received 10 August 2016; accepted 15 December 2016; published online 3 January 2017)

The electronic structure of bilayer graphene, where one of the layers possesses monovacancies, is studied under an external electric field using density functional theory. Our calculations show that Fermi-level pinning occurs in the bilayer graphene with defects under hole doping. However, under electron doping, the Fermi level rapidly increases at the critical gate voltage with an increasing electron concentration. In addition to the carrier species, the relative arrangement of the gate electrode to the defective graphene layer affects the Fermi energy position with respect to the carrier concentration. Because the distribution of the accumulated carrier depends on the electrode position, the quantum capacitance of bilayer graphene with defects depends on the electrode position.

Published by AIP Publishing. [<http://dx.doi.org/10.1063/1.4973426>]

Graphene has been attracting much attention in the applied sciences, especially in electronic device engineering, because of its unique structural and electronic properties. A bipartite network of C atoms with atomic thickness causes pairs of linear dispersion bands at the Fermi level that lead to an unusual quantum Hall effect and peculiar non-bonding π states at its edges.^{1,2} The linear dispersion bands near the Fermi level also cause a remarkable carrier mobility of up to $200\,000\text{ cm}^2/\text{Vs}$,³ which makes graphene an emerging material for high-speed electronic devices in the next generation. However, because of the absence of a band-gap, owing to the linear bands, graphene shows an intrinsic leakage current in the off state, which limits its usage in logic circuit applications. In addition, the electronic property of graphene is sensitive to external conditions such as electric field,^{4–7} atom/molecule absorption,⁸ atomic defects,^{9–12} topological defects,^{13,14} and interactions with other graphene sheets or substrates.^{15–21} Therefore, many studies have focused on developing methods to control the electronic structure of graphene. In particular, band-gap engineering has attracted much attention for realizing graphene-based semiconductor electronic devices. Many theoretical and experimental studies have reported a number of graphene derivatives having a large band-gap, such as graphene nanoribbons,²² a graphene nanomesh,²³ functionalized graphene,^{24–26} bilayer graphene under an external electric field,^{4,5,7} or molecular-doped bilayer graphene.²⁷

In our previous works,^{28,29} we demonstrated that a combination of the interlayer interaction and atomic defects could modulate the electronic structure of graphene thin films resulting in a finite energy gap in their π electron states, even though one or more layers of the thin films retain the perfect hexagonal network: For bilayer graphene, where one of the layers possesses the atomic and topological defects, our calculations showed that the bilayer graphene no longer possesses pairs of linear dispersion bands near the Fermi level, but has quadratic dispersion bands together with the

flat bands associated with the defects, even though one of the two layers retains its hexagonal atomic network. The energy gap between the top and the bottom of the π states belonging to the pristine layer strongly depends on the defect species and arrangement.

Although our findings indicate a possible procedure for realizing semiconducting graphene thin films, it is still unclear whether the electronic structure of the thin films with defects is controllable by an external electric field. Thus, in this work, we aim to provide further theoretical insight into the effect of defects on the electronic structures of bilayer graphene one of which layers possesses monovacancies (MVs) under carrier injection by the external electronic field, using first principles total energy calculations combined with the effective screening medium method. Our calculations show that the Fermi level is insensitive to the external electric field for hole injection, irrespective of the mutual arrangement of the gate electrode. In contrast, for electron doping, the Fermi level is rapidly shifted upward above the critical gate voltage, depending on the relative arrangement of the gate electrode to the defective layer. Furthermore, the electronic structure of the bilayer graphene does not exhibit a ridged band nature with respect to the excess carriers injected by the gate electrode. Defect-induced states are found to be sensitive to the carrier concentration, leading to the unusual electronic properties of bilayer graphene under an electric field.

All calculations were performed within the framework of density functional theory^{30,31} implemented into the STATE package.³² We used the local density approximation^{33,34} to describe the exchange-correlation potential among the interacting electrons. An ultrasoft pseudopotential generated by the Vanderbilt scheme was used to describe the interaction between electrons and ions.³⁵ The valence wave functions and charge density were expanded in terms of the plane-wave basis set with cutoff energies of 25 and 225 Ry, respectively. We adopted the effective screening medium (ESM) method to solve the Poisson equation including the external electric field.³⁶ The Brillouin-zone integration was performed with the

^{a)}E-mail: kkishimoto@comas.frsc.tsukuba.ac.jp

^{b)}E-mail: sokada@comas.frsc.tsukuba.ac.jp

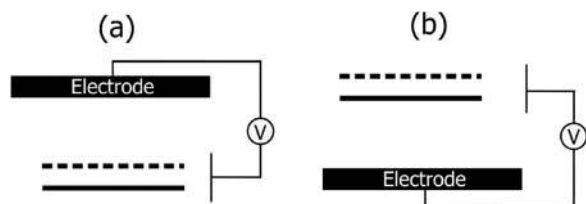


FIG. 1. Structural models of bilayer graphene with MV under an electric field with (a) a top gate and (b) a bottom gate. The dotted line represents the graphene layer with MV.

Γ -centered $8 \times 8 \times 1$ uniform k -mesh for self-consistent electronic structure calculations, which corresponds to the $32 \times 32 \times 1$ k -mesh in a primitive 1×1 cell of graphene, resulting in sufficient convergence for the geometric and electronic structures. All atoms were fully optimized until the remaining force acting on each atom was less than $0.005 \text{ Ry}/\text{\AA}$ under a fixed lateral lattice constant of 9.83 \AA corresponding to the experimental value of 4×4 lateral cell of graphene to avoid the over binding of the covalent bonds of C atoms.

In the present work, we consider bilayer graphene one of which layers possesses MV per 4×4 lateral unit cell of pristine graphene. Although the lateral lattice parameter is modulated by introducing the MV, we fixed the lateral parameter as 9.83 \AA to satisfy the commensurability condition between pristine and defective layers. Bilayer graphene has an AB stacking arrangement with an interlayer spacing of 3.4 \AA . During the calculations under a finite electric field, the atomic structure of the bilayer graphene with MV is fixed as the optimized structure obtained under the zero electric field. Electrons and holes were injected by a planar electrode situated above and below the bilayer graphene with a vacuum spacing of 5.8 \AA , mimicking the graphene field effect transistor with top and bottom gate electrodes, respectively, with respect to the defective layer, as shown in Fig. 1. The electrode is simulated by an effective screening medium with an infinite relative permittivity.

Figure 2 shows the Fermi level of bilayer graphene, one of which layers possesses MV, as a function of the gate

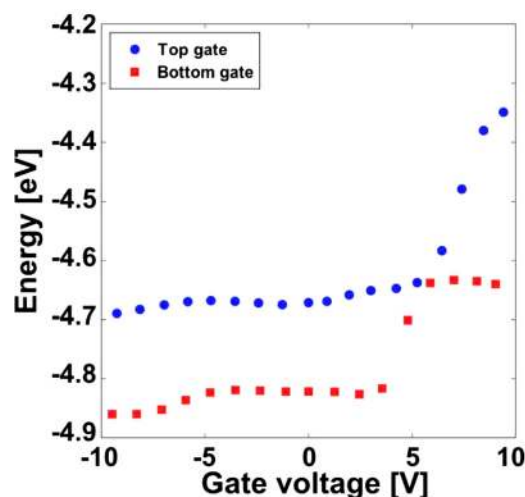


FIG. 2. Fermi energy of bilayer graphene with MV as a function of the gate voltage. Blue circles and red squares show the results of the top gate and bottom gate, respectively. Electron and hole injections correspond to the positive and negative gate voltage, respectively.

voltage. The Fermi level is insensitive to the negative gate voltage or hole concentration: The Fermi level retains an almost constant value up to a gate voltage of -10 V irrespective of the gate arrangements, indicating that the Fermi level is pinned at approximately -4.7 and -4.8 eV for the top and bottom gate arrangements, respectively. Therefore, under a low hole concentration, a carrier is hardly injected into the bilayer graphene with defects. In contrast, for a positive gate voltage, corresponding to electron doping, the Fermi level is sensitive to the electron concentration: First, the Fermi level retains an almost constant value up to the gate voltage of 5.2 and 3.6 V for the top and bottom gate arrangements, respectively, and then it rapidly shifts upward with increasing gate voltage. Therefore, a positive gate voltage can tune the electronic structure of bilayer graphene with defects.

To provide physical insight into the unusual gate voltage dependence of the Fermi level, we depict the electronic energy band and density of states (DOS) of the bilayer graphene under an electric field applied by the top and bottom gate electrodes together with the electronic structure and squared wave function of the bilayer graphene without an external field (Fig. 3). Note that the graphene with MV exhibits spin polarization around the defect.⁹ Furthermore, the optimized structure studied here is also different from that reported in the literature.⁹ Thus, the present electronic structure is slightly different from that of the geometry obtained by the spin-polarized calculations. For the bilayer graphene without the field, three flat dispersion bands emerge in the energy gap of the dispersive π electron states [Fig. 3(a)]. The upper two states are associated with the unsaturated σ state of dangling bonds at the vacancy, which are localized at the edge atomic site of the vacancy [d_1 and d_2 states in Fig. 3(a)]. In contrast, the lowest branch of the flat bands has a non-bonding π state caused by the MV, exhibiting an extended nature [the d_3 state in Fig. 3(a)]. The wave function distribution of these three states clarifies the physical mechanism of the unusual field dependence of the Fermi level. For hole doping, the holes are injected into the flat band states associated with the defect states possessing a non-bonding π nature. Because of its flat band nature, the state leads to a large peak in the DOS, which prevents the shift of the Fermi level by injecting the hole into this state. For electron doping, even though the σ dangling bond states cause a large DOS in the energy gap of the π states, the localized nature of the state causes a rapid upward shift by the electron doping, because of the large on-site Coulomb interaction in these states.

The electronic band structure of the bilayer graphene with defects under an external electric field depends on the carrier species, carrier concentration, and relative electrode arrangement, indicating that the ridged band nature is not retained upon carrier injection. For the electron doping, owing to the upward shift of the d_1 and d_2 states associated with the σ dangling bonds at the defects, the band width of the three defect states increases with increasing electron concentration. In particular, for the top gate electrode arrangement, the lowest defect state with non-bonding π nature is separated from the remaining two states with dangling bond σ states. Thus, the electronic structure near the Fermi level is highly modulated by the electron doping, depending on the

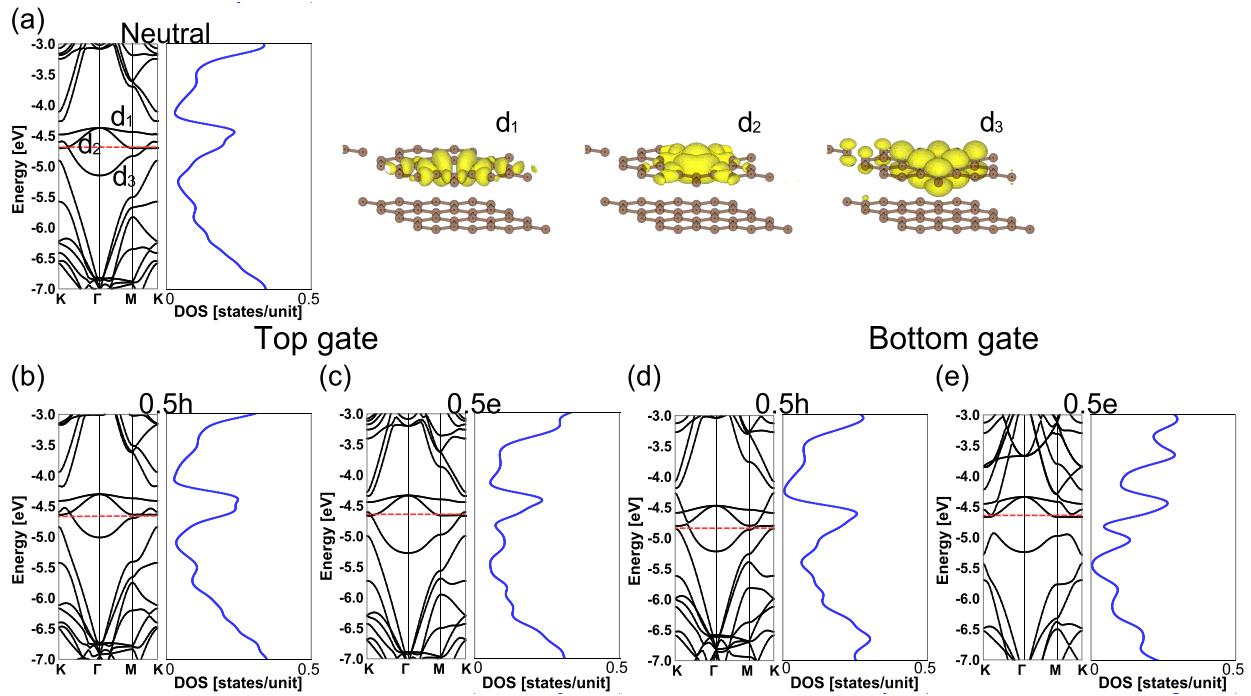


FIG. 3. (a) Electronic energy band and DOS of bilayer graphene with MV without an external electric field. The dotted line shows the Fermi level. The three right panels of the figure show the isosurfaces of the wave function of the three states near the Fermi level denoted by d_1 , d_2 , and d_3 . The electronic energy band and DOS of bilayer graphene with MV under a gate voltage of (b) -5.8 V from the top gate (which corresponds to a 0.5 hole injection per unit cell), (c) 5.2 V from the top gate (which corresponds to a 0.5 electron injection per unit cell), (d) -5.9 V from the bottom gate (which corresponds to a 0.5 hole injection per unit cell), and (e) 5.8 V from the bottom gate (which corresponds to a 0.5 electron injection per unit cell). Dotted lines represent the Fermi level.

gate arrangements. In contrast, the electronic states associated with the defect states are relatively insensitive to the hole doping compared with the electron doping. In this case, the band structure mainly depends on the relative position of the gate electrode.

Because the electronic energy band of the bilayer graphene one of which layers possesses MV is sensitive to the carrier concentration and the relative arrangement of the gate electrode; the accumulated carriers also depend on the relative position of the gate electrode to the defects. Figure 4 shows the isosurfaces of the accumulated carriers under an external electric field. For electron doping with the bottom gate arrangement, the accumulated carrier exhibits an extended nature compared with the other carrier species and gate arrangement: Accumulated electrons are distributed mainly on the layer situated on the electrode side. In addition, the electrons are also localized around the σ dangling bond states on the other layer with defects. In contrast, for the other situations, the accumulated carriers are distributed on the layer situated on the electrode side irrespective of the carrier species.

Characteristic distributions of the accumulated carriers imply that the quantum capacitance of the bilayer graphene

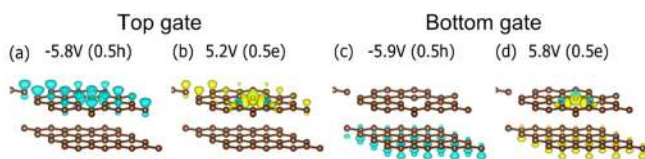


FIG. 4. Isosurfaces of the accumulated carrier by carrier injection under a gate voltage of (a) -5.8 V ($0.5h$) from the top gate, (b) 5.2 V ($0.5e$) from the top gate, (c) -5.9 V ($0.5h$) from the bottom gate, and (d) 5.8 V ($0.5e$) from the bottom gate.

one of which layers possesses MV, with respect to the gate electrode, is also sensitive to the gate arrangement and carrier species. Figure 5 shows the capacitance of bilayer graphene with MV as a function of the gate voltage. The capacitance of the bilayer graphene depends on the gate voltage and mutual electrode arrangement to the defect. For hole doping, the capacitance remains at an almost constant value of 0.016 aF/nm², because the sufficiently large density of states can accommodate an excess of holes into the graphene layer situated at the electrode side. For electron doping, the capacitance of the bilayer graphene with the bottom

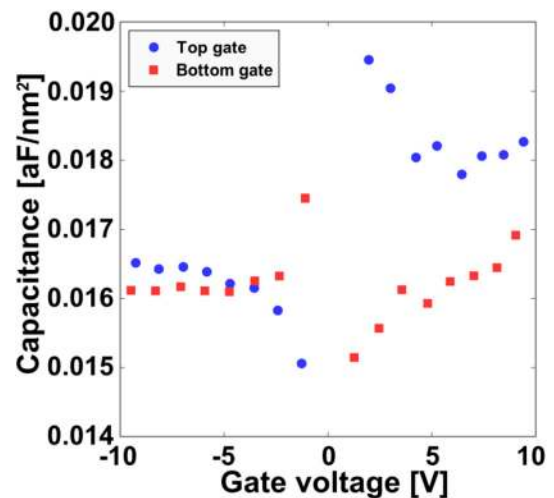


FIG. 5. Capacitance of bilayer graphene with MV as a function of the gate voltage. Blue circles and red squares show the results of the top gate and bottom gate, respectively. Electron and hole injections correspond to the positive and negative gate voltage, respectively.

gate arrangement is smaller than that with the top gate arrangement, because the electrons in the bilayer graphene with the bottom gate arrangement spill over to the second graphene layer possessing the defects.

Note that the MV does not show the pentagonal reconstruction but possesses a trigonal structure as its metastable conformation, according to the constraint on the lateral lattice constant ([supplementary material](#)). However, the model considered here is sufficient to discuss whether the defect induced states affect the carrier accumulation by the external electric field or not, except the detailed electronic structure at the Fermi level [Fig. S1]. Indeed, the Fermi level is pinned upon the hole injection, while it shifts upward upon the electron injection [Fig. S2]. Furthermore, the distribution of the accumulated carrier is the same as that of the bilayer graphene with trigonal MV. For electron doping with the bottom gate arrangement, accumulated electrons are distributed mainly on the layer situated on the electrode side together with the spilled carriers localized around the σ dangling bond states at the defects. In contrast, for the top gate situation, the accumulated carriers are distributed on the layer situated on the electrode side irrespective of the carrier species [Fig. S3].

See [supplementary material](#) for electronic properties of bilayer graphene with reconstructed defects.

This work was supported by CREST, from the Japan Science and Technology Agency, JSPS KAKENHI Grant Nos. JP25246010, JP16H00898, and JP16H06331 from Japan Society For the Promotion of Science, and the Joint Research Program on Zero-Emission Energy Research, Institute of Advanced Energy, Kyoto University. Part of the calculations was performed on an NEC SX-Ace at the Cybermedia Center at Osaka University and on an SGI ICE XA/UV at the Institute of Solid State Physics, The University of Tokyo.

¹K. S. Novoselov, A. K. Geim, S. V. Morozov, D. Jiang, M. I. Katsnelson, I. V. Grigorieva, S. V. Dubonos, and A. A. Firsov, *Nature* **438**, 197 (2005).

²Y. Zhang, Y.-W. Tan, H. L. Stormer, and P. Kim, *Nature* **438**, 201 (2005).

³K. I. Bolotin, K. J. Sikes, Z. Jiang, M. Klima, G. Fudenberg, J. Hone, P. Kim, and H. L. Stormer, *Solid State Commun.* **146**, 351 (2008).

⁴J. B. Oostinga, H. B. Heersche, X. Liu, A. F. Morpurgo, and L. M. K. Vandersypen, *Nat. Mater.* **7**, 151 (2007).

⁵Y. Zhang, T. Tang, C. Girit, Z. Hao, M. C. Martin, A. Zettl, M. F. Crommie, Y. R. Shen, and F. Wang, *Nature* **459**, 820 (2009).

⁶M. F. Craciun, S. Russo, M. Yamamoto, J. B. Oostinga, A. F. Morpurgo, and S. Tarucha, *Nat. Nanotechnol.* **4**, 383 (2009).

⁷S. Konabe and S. Okada, *J. Phys. Soc. Jpn.* **81**, 113702 (2012).

⁸R. Balog, B. Jørgensen, L. Nilsson, M. Andersen, E. Rienks, M. Bianchi, M. Fanetti, E. Lægsgaard, A. Baraldi, S. Lizzit, Z. Sljivancanin, F. Besenbacher, B. Hammer, T. G. Pedersen, P. Hofmann, and L. Høneker, *Nat. Mater.* **9**, 315 (2010).

⁹Y. Ma, P. O. Lehtinen, A. S. Foster, and R. M. Nieminen, *New J. Phys.* **6**, 68 (2004).

¹⁰H. Amara, S. Latil, V. Meunier, Ph. Lambin, and J.-C. Charlier, *Phys. Rev. B* **76**, 115423 (2007).

¹¹M. M. Ugeda, I. Brihuega, F. Hiebel, P. Mallet, J.-Y. Veuillen, J. M. G.-Rodriguez, and F. Yndurain, *Phys. Rev. B* **85**, 121402(R) (2012).

¹²M. Dvorak, W. Oswald, and Z. Wu, *Sci. Rep.* **3**, 2289 (2013).

¹³P. Koskinen, S. Malola, and H. Häkkinen, *Phys. Rev. Lett.* **101**, 115502 (2008).

¹⁴S. Okada, T. Kawai, and K. Nakada, *J. Phys. Soc. Jpn.* **80**, 013709 (2011).

¹⁵S. Y. Zhou, G.-H. Gweon, A. V. Fedorov, P. N. First, W. A. de Heer, D.-H. Lee, F. Guinea, A. H. C. Neto, and A. Lanzara, *Nat. Mater.* **6**, 770 (2007).

¹⁶A. Mattheis and O. Pankratov, *Phys. Rev. Lett.* **99**, 076802 (2007).

¹⁷N. T. Cuong, M. Otani, and S. Okada, *Phys. Rev. Lett.* **106**, 106801 (2011).

¹⁸K. Kamiya, N. Umezawa, and S. Okada, *Phys. Rev. B* **83**, 153413 (2011).

¹⁹M. Koshino and T. Ando, *Phys. Rev. B* **76**, 085425 (2007).

²⁰M. Otani, M. Koshino, Y. Takagi, and S. Okada, *Phys. Rev. B* **81**, 161403(R) (2010).

²¹W. Bao, L. Jing, J. Velasco, Jr., Y. Lee, G. Liu, D. Tran, B. Standley, M. Aykol, S. B. Cronin, D. Smirnov, M. Koshino, E. McCann, M. Bockrath, and C. N. Lau, *Nat. Phys.* **7**, 948 (2011).

²²K. Nakada, M. Fujita, G. Dresselhaus, and M. S. Dresselhaus, *Phys. Rev. B* **54**, 17954 (1996).

²³T. G. Pedersen, C. Flindt, J. Pedersen, N. A. Mortensen, A. P. Jauho, and K. Pedersen, *Phys. Rev. Lett.* **100**, 136804 (2008).

²⁴J. O. Sofo, A. S. Chaudhari, and G. D. Barber, *Phys. Rev. B* **75**, 153401 (2007).

²⁵J. Zhou, M. M. Wu, X. Zhou, and Q. Sun, *Appl. Phys. Lett.* **95**, 103108 (2009).

²⁶F. Withers, T. H. Bointon, M. Dubois, S. Russo, and M. F. Craciun, *Nano Lett.* **11**, 3912 (2011).

²⁷N.-T. Cuong, M. Otani, and S. Okada, *Appl. Phys. Lett.* **101**, 233106 (2012).

²⁸K. Kishimoto and S. Okada, *Surf. Sci.* **644**, 18 (2016).

²⁹K. Kishimoto and S. Okada, *Jpn. J. Appl. Phys., Part 1* **55**, 06GF06 (2016).

³⁰P. Hohenberg and W. Kohn, *Phys. Rev.* **136**, B864 (1964).

³¹W. Kohn and L. J. Sham, *Phys. Rev.* **140**, A1133 (1965).

³²Y. Morikawa, K. Iwata, and K. Terakura, *Appl. Surf. Sci.* **169–170**, 11 (2000).

³³J. P. Perdew and A. Zunger, *Phys. Rev. B* **23**, 5048 (1981).

³⁴D. M. Ceperley and B. J. Alder, *Phys. Rev. Lett.* **45**, 566 (1980).

³⁵D. Vanderbilt, *Phys. Rev. B* **41**, 7892 (1990).

³⁶M. Otani and O. Sugino, *Phys. Rev. B* **73**, 115407 (2006).